Superresolved digital in-line holographic microscopy for high-resolution lensless biological imaging

Vicente Micó
Universitat de Valencia
Departamento de Óptica
C/Dr. Moliner 50
46100 Burjassot, Spain

Zeev Zalevsky
Bar-Ilan University
School of Engineering
Ramat-Gan 52900, Israel

Abstract. Digital in-line holographic microscopy (DIHM) is a modern approach capable of achieving micron-range lateral and depth resolutions in three-dimensional imaging. DIHM in combination with numerical imaging reconstruction uses an extremely simplified setup while retaining the advantages provided by holography with enhanced capabilities derived from algorithmic digital processing. We introduce superresolved DIHM incoming from time and angular multiplexing of the sample spatial frequency information and yielding in the generation of a synthetic aperture (SA). The SA expands the cutoff frequency of the imaging system, allowing submicron resolutions in both transversal and axial directions. The proposed approach can be applied when imaging essentially transparent (low-concentration dilutions) and static (slow dynamics) samples. Validation of the method for both a synthetic object (U.S. Air Force resolution test) to quantify the resolution improvement and a biological specimen (sperm cells biosample) are reported showing the generation of high synthetic numerical aperture values working without lenses. © *2010 Society of Photo-Optical Instrumentation Engineers.* [DOI: 10.1117/1.3481142]

Keywords: holography; digital recording; microscopy; digital imaging; synthetic apertures; resolution.

Paper 10078R received Feb. 13, 2010; revised manuscript received Jun. 28, 2010; accepted for publication Jul. 1, 2010; published online Aug. 19, 2010.

1 Introduction

History of digital in-line holographic microscopy (DIHM) (or lensless microscopy) started when Gabor reported on a method to avoid spherical aberration, improving image quality in electron microscopy by preventing lenses in the experimental setup.[1] In this in-line configuration, the nondiffracted light acts as reference beam that interferes with the diffracted components generated by the sample. If the object blocks only a small part of the illumination beam (that is, the object can be considered as a weak diffractive sample) then reconstruction of the complex amplitude that is diffracted by the object is feasible by using holographic tools. On the other hand, when the object blocks a high amount of light, reconstruction by Gabor's concept is not applicable because diffraction dominates the process and other strategies are needed to retrieve the diffracted object's wavefront information.[2,3]

Nevertheless, weak diffractive samples are quiet common in biomedical imaging practice because many are low-concentration samples, or single-cell samples, or thick quasi-transparent samples, etc. For this reason, the original idea reported by Gabor[1] has been recently revived in the optical range coinciding with the relatively modern developments in both solid-state image sensors and numerical processing capabilities provided by computers.[4,5] The use of DIHM in biology have enables 3-D imaging with resolution in the micrometer range in applications such as underwater observations, tracking of moving objects and particles, identification of microorganisms, and the study of erosion processes in coastal sediments.[6–9]

However, DIHM lacks high numerical aperture (NA) due to both geometrical distortion and the mandatory compromise between the illumination pinhole diameter, the illumination wavelength, and the need to obtain a reasonable light efficiency. Thus, achievable NA values in DIHM are typically around 0.45,[10] and ways to improve the NA are of unquestionable interest. One can identify two different types of approaches aimed to improve the NA in DIHM: approaches involving modifications in the DIHM setup (first class) and those involving improvements in the numerical reconstruction procedure (second class).

As an example of first class of methods, Garcia-Sucerquia et al. reported on a clever way to improve the NA of the DIHM setup.[11] They replaced the air gap between the input sample and the CCD by a high refractive index medium. This strategy directly increases the NA value because the refractive index of the surrounding medium explicitly defines the NA. Garcia-Sucerquia et al.[11] achieved an improvement in the NA value from 0.39 to 0.55. And as second one, Kanka et al. have recently proposed two approaches to provide high-contrast, high-resolution images in DIHM based on the so-called tile superposition propagation (TSP) technique.[12,13] Essentially, the TSP method is a fast propagation algorithm involving low-computer-memory consumption for exact scalar wave field propagation. The TSP algorithm divides the recorded ho-
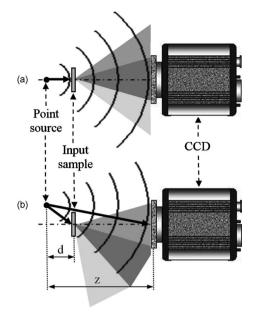
Fig. 1 Sketch of the SR DIHM setup: (a) on-axis and (b) off-axis illumination cases.

logram into a set of tiles having the same size, processes the tiles separately using conventional numerical propagation methods, and adds all the propagated tiles into a single one. Using this strategy, Kanka et al.[12,13] have demonstrated imaging capabilities in DIHM with resolutions corresponding with NA values between 0.6 and 0.7.

In this paper, we present a first-class technique (according to our previous classification) that improves the resolution in DIHM by means of the generation of a synthetic aperture (SA) while maintaining the simplicity of DIHM concept. The SA generation is based on the combination of angular multiplexing provided by tilted beam illumination with time multiplexing of a different object's spectral regions. This strategy has been successfully used to improve the NA value of imaging systems.[14]

Briefly, different spectral regions of the object's spectrum are multiplexed in different domains according to a given *a priori* knowledge about the input object. The multiplexing allows the passage of different bandpass images having different spatial-frequency content through the aperture limited system. A holographic recording is commonly used to recover each additional elementary aperture in order to synthesize an expanded SA. Using this strategy, synthetic NA (SNA) above the theoretical limit for air-immersed imaging systems has been reported in the literature,[15,16] while more modest values have been validated in digital lensless Fourier holography.[17,18] The generation of a SA also improves the axial resolution, making it possible to increase the optical sectioning of the imaging system.[19]

2 Methodology

Here, we will report on the implementation of time and angular multiplexing in DIHM and demonstrate the generation of a SA having a high SNA value. The experimental setup is depicted in Fig. 1. Because of the low divergence of commercially available diode lasers, high NA DIHM needs focaliza-

tion of the laser beam to achieve high-NA spherically divergent point-source illumination. Thus, two alternatives can be implemented. On the one hand, we can use an objective lens adapted to a pinhole having a diameter close to the illumination wavelength (λ), and on the other hand, we can use only a high NA objective lens. In any case, a divergent spherical wave illuminates the sample and a CCD device records the geometrically magnified diffraction pattern [Fig. 1(a)]. In that in-line hologram, the system lateral magnification (M) depends on both the point source–to-object distance (d) and the point source–to-CCD distance (z); that is, $M = z/d$. Also, the resolution limit (R) can be defined as $R = \lambda/\text{NA}$, where NA is that of the CCD device when it is seen from the axial object point. As an example, the resolution limit is 0.88 μm when considering a 0.46 NA and 405 nm violet laser light.[10]

However, it is possible to further improve those values by considering SA generation strategies. Here, the point source is shifted to several off-axis positions in order to provide different tilted beam illuminations over the input sample. The shifting distance (s) of the point source is then adjusted with both the distance d and the NA of the imaging system (NA_{CCD}) in order to provide an illumination angle that doubles the one provided by NA_{CCD}. Obviously, the point source NA must be high enough to allow this condition. Thus, the object becomes obliquely illuminated and will generate on-axis diffraction of additional spectral portions. This new spectral content interferes with the nondiffracted light of the illumination beam that passes through the sample without being distorted because we are under Gabor assumptions [Fig. 1(b)]. And, to satisfy the Nyquist sampling criterion in the digitally recorded hologram, the s distance must fulfill the paraxial condition given by $s_m \leq \lambda z/2p$, where p is the pixel size of the CCD device and s_m the maximum distance that the point source can be shifted.

After angular multiplexing the object's spectrum with different sequential tilted beam illuminations, each recorded hologram is numerically processed to synthesize the expanded SA. The digital manipulation implies: (*i*) A coordinate transformation to remove the nonlinear geometrical distortion incoming from the violation of the Fresnel approximation,[2,4] (*ii*) an input plane numerical backpropagation that can be achieved by implementing the convolution approach in the Rayleigh-Sommerfeld equation,[2,3,16] and (*iii*) a correct reallocation of the spectral content of each bandpass image while generating the SA.[16,18] Finally, the SR image is obtained by Fourier transforming the information contained in the SA.

3 Experimental Investigation

Different experimental results are reported in the experimental validation of the proposed method. In the first experiment, we propose the use of a vertical cavity surface emitting laser (VCSEL) source as illumination light ($\lambda = 0.85$ μm). In order to calibrate the setup, a positive high-resolution U.S. Air Force (USAF) test target is used as input object. A CCD camera (Basler A312f, 582×782 pixels, 8.3 pixel size, 12 bits/pixel) is used to record the holograms. The VCSEL source is placed onto a motorized linear translation stage to allow off-axis displacement. A commercial grade standard microscope lens (DIN 40x, 0.65NA) is used to provide high NA illumination in the setup. The point source–test and point
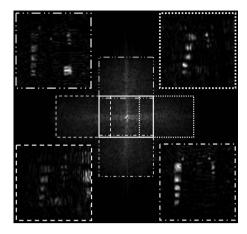
Fig. 2 Generated SA in the VCSEL point source illumination case coming from the addition of four off-axis elementary apertures. At the corners are the four bandpass images used in the SA generation.

source–CCD distances are $d = 400$ μm and $z = 11.4$ mm, respectively. The point source is shifted 175 μm (s distance) from the optical axis to allow four off-axis recordings in the vertical (V) and horizontal (H) orthogonal directions.

Note that this distance is lower than the one defined by the Nyquist criterion ($s_m = 0.563 \mu$m) and it is the proper distance to transmit quasi-contiguous spectral content in the shorter (V) CCD direction. As result, the NA of the tilted illumination is $NA_{ILUM} = 0.4$. Figure 2 images both the four recovered bandpass images when tilted beam illumination is performed and after applying the numerical reconstruction procedure, and the generated SA incoming from the addition of the four off-axis images with the central one (on-axis illumination case). Each bandpass image corresponds with an elementary rectangular aperture in the generated SA because they are denoted by different types of lines.

Figure 3 depicts the case of conventional DIHM [Fig. 3(a)] coming from the central rectangular aperture of Fig. 2, and SR DIHM [Fig. 3(b)] coming from the Fourier transformation of the expanded SA. As a result, the NA and SNA values for the V and H directions are improved from $NA_V = 0.21$ and $NA_H = 0.28$ to $SNA_V = 0.61$ and $SNA_H = 0.68$, respectively. Obviously, resolution limits are also improved according to those SNA values and can resolve, in both V and H directions, the last element of the USAF test (Group 9, Element 3 having a period of 1.55 μm). The three elements corresponding with Group 9 are magnified in Fig. 3(c) while a vertical section along the dashed black line in Fig. 3(c) is plotted in Fig. 3(d) to clearly show the three black lines integrating each one of the elements. However, despite of the generated high SNA value, the new superresolution limits are modest (>1 μm) because of the VCSEL illumination wavelength.

To validate resolution limits of <1 μm, we performed a second experiment in which a violet laser ($\lambda = 0.405$ μm) is used. The experimental setup configuration is the same one as before. Once again, the condition imposed by the Nyquist maximum shift ($s_m = 0.268$ μm for violet wavelength) is still fulfilled. Figure 4(a) depicts the case when conventional DIHM is considered. Because the illumination wavelength of the violet laser is 2.1 times lower than that of VCSEL, 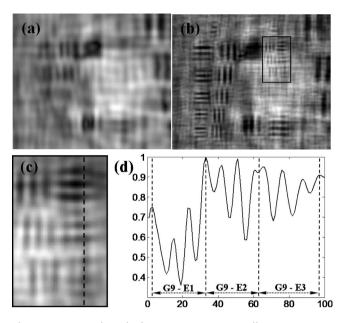the resolution limits become improved while the NA values remain constant. According to the theory, the new superresolution limits are $SR_V = 0.66$ μm and $SR_H = 0.59$ μm incoming from $SNA_V = 0.61$ and $SNA_H = 0.68$, respectively. However, aside from a global improvement in the image quality, there are not enough elements in the test to quantify the superresolution effect when SR DIHM is applied [Fig. 4(b)]. Thus, we have applied our method to a biological sample: it is an unstained swine sperm biosample that is dried up allowing fixed sperm cells for the experiments. The sperm cells have an ellipsoidal head of 6×9 μm and a tail's width of ~ 2 μm on the head side and <1 μm on its end. Figure 5 shows the experimental results. Now, not only four off-axis elementary

Fig. 3 Experimental results for VCSEL point source illumination case: (a) reconstructed image using conventional DIHM, (b) reconstructed image using SR DIHM approach, (c) magnified area corresponding with the rectangle in (b), and (d) normalized cross section along the dashed line in (c).
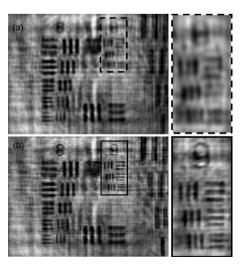

Fig. 4 Experimental results for violet laser point source and USAF test: (a) reconstructed image using conventional DIHM and (b) reconstructed image using SR DIHM approach.
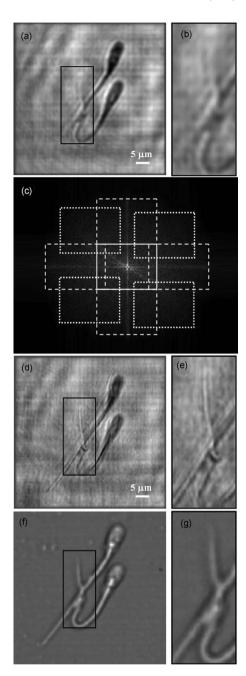
Fig. 5 Experimental results for violet laser point source and sperm cells biosample: (a) reconstructed image using conventional DIHM, (c) generated SA from the addition of eight off-axis elementary apertures, (d) reconstructed image using SR DIHM approach, and (f) reference image (0.8 NA objective lens) under spatially coherent broadband illumination. Images in (b), (e), and (f) are magnified areas of the black rectangles included in (a), (d), and (f), respectively.

apertures are considered, but eight are, as we can see in the generated SA [Fig. 5(c)]. Thus, full two-dimensional spatial frequency space is covered in the SA. We can observe that the thinner part of the tail, which is not visible under conventional DIHM [Figs. 5(a) and 5(b)], becomes resolved after applying the proposed SR DIHM approach [Figs. 5(d) and 5(e)]. Finally, Figs. 5(f) and 5(g) show a reference image of the same biosample area taken with a 0.8 NA, 60x microscope lens

from a BX61 Olympus microscope under spatially coherent (closing the condenser diaphragm) white-light illumination.

4 Conclusions

In this paper, we have introduced and validated SR DIHM as a lensless microscopic imaging method that is based on SA generation incoming from tilted beam illumination over the input sample and holographic recording. The experimental setup becomes extremely simple and verifies the definition of a SNA of being larger than 0.6 in every direction. This NA value obtained when considering the proposed approach is comparable to the maximum achieved 0.7 NA reported in the field of DIHM.[12] The full procedure can be realized in a few seconds by automating the displacement of the source to the off-axis positions and synchronizing the capture of the holograms. We have calibrated and quantified the method using a standard USAF resolution test target achieving a submicron resolution limit.

We have also reported on the application of the proposed approach to imaging of a sperm cell biosample demonstrating its feasibility for the analysis of biological samples. The proposed approach can be applied for submicron resolution lensless imaging purposes when considering essentially transparent (low-concentration dilution) samples. Also, although the proposed approach is limited to samples that are static or has a slow variation in time (a few seconds), extension of the technique to nonstatic (fast dynamic) samples is under consideration.

References

1. D. Gabor, "A new microscopic principle," *Nature* **161**(4098), 777–778 (1948).
2. Y. Takaki and H. Ohzu, "Fast numerical reconstruction technique for high-resolution hybrid holographic microscopy," *Appl. Opt.* **38**(11), 2204–2211 (1999).
3. V. Micó, J. García, Z. Zalevsky, and B. Javidi, "Phase-shifting Gabor holography," *Opt. Lett.* **34**(10), 1492–1494 (2009).
4. W. Xu, M. H. Jericho, I. A. Meinertzhagen, and H. J. Kreuzer, "Digital in-line holography for biological applications," *Proc. Natl. Acad. Sci. U.S.A.* **98**(20), 11301–11305 (2001).
5. L. Repetto, E. Piano, and C. Pontiggia, "Lensless digital holographic microscope with light-emitting diode illumination," *Opt. Lett.* **29**(10), 1132–1134 (2004).
6. P. R. Hobson and J. Watson, "The principles and practice of holographic recording of plankton," *J. Opt. A, Pure Appl. Opt.* **4**(4), S34–S49 (2002).
7. W. Xu, M. H. Jericho, I. A. Meinertzhagen, and H. J. Kreuzer, "Tracking particles in 4-D with in-line holographic microscopy," *Opt. Lett.* **28**(3), 164–166 (2003).
8. J. Garcia-Sucerquia, W. Xu, S. K. Jericho, P. Klages, M. H. Jericho, and H. J. Kreuzer "Digital in-line holographic microscopy," *Appl. Opt.* **45**(5), 836–850 (2006).
9. N. Verrier, S. Coëtmellec, M. Brunel, D. Lebrun, and A. J. E. M. Janssen, "Digital in-line holography with an elliptical, astigmatic Gaussian beam: wide-angle reconstruction," *J. Opt. Soc. Am. A* **25**(6), 1459–1466 (2008).
10. J. Garcia-Sucerquia, D. C. Alvarez-Palacio, M. H. Jericho, and H. J. Kreuzer, "Comment on reconstruction algorithm for high-numerical-aperture holograms with diffraction-limited resolution," *Opt. Lett.* **31**(19), 2845–2847 (2006).

11. J. Garcia-Sucerquia, W. Xu, M. H. Jericho, and H. J. Kreuzer, "Immersion digital in-line holographic microscopy," *Opt. Lett.* **31**(9), 1211–1213 (2006).

12. M. Kanka, R. Riesenberg, and H. J. Kreuzer, "Reconstruction of high-resolution holographic microscopic images," *Opt. Lett.* **34**(8), 1162–1164 (2009).

13. M. Kanka, A. Wuttig, C. Graulig, and R. Riesenberg, "Fast exact scalar propagation for an in-line holographic microscopy on the diffraction limit," *Opt. Lett.* **35**(2), 217–219 (2010).

14. V. Micó, Z. Zalevsky, and J. García, "Optical superresolution: imaging beyond Abbe's diffraction limit," *J. Holography Speckle* **5**(2), 110–123 (2009).

15. Y. Kuznetsova, A. Neumann, and S. R. J. Brueck, "Imaging interferometric microscopy—approaching the linear systems limits of optical resolution," *Opt. Express* **15**(11), 6651–6663 (2007).

16. V. Micó, Z. Zalevsky, C. Ferreira, and J. García, "Superresolution digital holographic microscopy for three-dimensional samples," *Opt. Express* **16**(23), 19260–19270 (2008).

17. C. Yuan, H. Zhai, and H. Liu, "Angular multiplexing in pulsed digital holography for aperture synthesis," *Opt. Lett.* **33**(20), 2356–2358 (2008).

18. L. Granero, V. Micó, Z. Zalevsky, and J. García, "Synthetic aperture superresolved microscopy in digital lensless Fourier holography," *Appl. Opt.* **49**(5), 845–857 (2010).

19. V. Micó, J. García, and Z. Zalevsky, "Axial superresolution by synthetic aperture generation," *J. Opt. A, Pure Appl. Opt.* **10**(12), 125001 (2008).